Arab J Geosci (2016) 9: 405
DOI 10.1007/s12517-016-2413-y

ORIGINAL PAPER

Fault-controlled, bedding-parallel dolomite in the middle Jurassic Samana Suk Formation in Margalla Hill Ranges, Khanpur area (North Pakistan): petrography, geochemistry, and petrophysical characteristics

Mumtaz Muhammad Shah[1,4] · **Waqar Ahmed**[2] · **Naveed Ahsan**[3] · **Mona Lisa**[4]

Received: 3 August 2015 / Accepted: 26 February 2016 / Published online: 3 May 2016

Abstract This study deals with superb fault-controlled, bedding-parallel dolomite in the shallow marine platform carbonates of the Samana Suk Formation (middle Jurassic), southern Hazara basin, NW Pakistan. Field observations, petrographic studies, mineralogical and isotopic analyses, and porosity-permeability analyses allow to unravel the diagenetic evolution of documented diagenetic phases and their impact on the reservoir behavior. Various diagenetic phases are recognized, which include (i) two episodes of replacive dolomites (Dol. I and Dol. II), (ii) initial phase of white calcite cement (WC-I), (iii) saddle dolomite (SD), (iv) late phase of white calcite cement (WC-II), and (v) transparent calcite cement (TC). In addition, other diagenetic features are bedding-parallel stylolites (PBSs), cataclastic deformation, and dissolution. Stable C- and O-isotope signatures confirmt that elevated temperature fluids resulted in the formation of the various dolomite and calcite phases. Porosity-permeability studies revealed enhanced porosity in the replacive dolomite (i.e., Dol. I and Dol. II), but late stage cementation in relation to calcite and dolomite cementation showed adverse effect on the reservoir quality. Furthermore, diagenetic alterations (i.e., brecciation and dissolution) along faults contributed in the enhancement of reservoir properties.

In conclusion, dolomitization occurred due to the percolation of Mg-rich fluids along the Haro Fault and its splays. Dewatering of basinal fluids from the underlying siliciclastic rocks or deep and hot hydrothermal fluids may be the possible source of dolomitization.

Keywords Replacive dolomite · O/C isotopic signatures · Saddle dolomite · Basinal fluids

This article is a part of Topical Collection on *Arabian Plate: Lithosphere Dynamics, Sedimentary Basins &; Geohazards*

✉ Mumtaz Muhammad Shah
mshah@qau.edu.pk

Waqar Ahmed
geowaqar89@yahoo.com

Naveed Ahsan
naveedahsan.geo@pu.edu.pk

Mona Lisa
lisa_qau@yahoo.com

[1] SE-Asia Carbonate Research Laboratory, Universiti Teknologi Petronas, 31750 Tronoh, Malaysia

[2] Department of Geology, University of Malakand, Lower Dir 18800, Pakistan

[3] Institute of Geology, University of the Punjab, Lahore 54590, Pakistan

[4] Department of Earth Sciences, Quaid-i-Azam University, Islamabad 45320, Pakistan

Introduction

During the last decades, the presence of dolomite associated with hydrocarbon reservoirs paved the way to extensive studies of dolomite bodies formed through different processes. Still, additional input data is needed to better understand the controlling factors that affect the rock heterogeneities in dolomite geo-bodies. Structurally controlled dolomite represents one of such dolomite that required more in-depth studies to explain associated replacement processes (Sharp et al. 2010). Various authors synthesized different characteristics of fault-related dolomite bodies, especially unravelling the fluid flow mechanism responsible dolomitization (Hendry et al. 2015; Martin-Martin et al. 2015; Vandeginste et al. 2014; Sharp et al. 2010; Lopéz-Horgue et al. 2010; Nader et al. 2009; Davies and Smith

2006; Gomez-Rivas et al 2014). In addition, relationship between diagenetic modifications that resulted in various dolomite phases and their impact on reservoir behavior has also been discussed (Dewit et al. 2012).

The distributions of dolomite geo-bodies generally follow the trends of the feeding faults (dolomitizing fluid pathway), but these geo-bodies prefer suitable beds (i.e., dolomitizing fluid flow along more permeable beds) as they move away from the fault and hence resulted into bedding-parallel dolomitization, also referred as "stratum-bound dolostones" (Martin-Martin et al. 2015; Sharp et al. 2010). In order to understand the development of various diagenetic phases in the bedding-parallel dolomites and their effects on the reservoir quality, detailed field analogue investigations are required. The present study focused on an excellently exposed fault-controlled, bedding-parallel dolomite bodies in the middle Jurassic Samana Suk Formation in the southern Hazara basin (NW Pakistan). This study reports on field investigations, petrographic studies, isotopic analyses, and porosity-permeability analyses. The aims of this study are to understand diagenetic modifications related to the fault-related Mg-rich fluid migration and to define the diagenetic modifications on the reservoir quality.

Tectonic setting

The successive processes of rifting and fragmentation of Gondwanaland resulted in the Paleo-Tethys Ocean during middle to late Paleozoic, which stretched from the Pacific to the Mediterranean encompassing India and the northern flanks of Arabia and Africa (Angiolini et al. 2003; Kazmi and Jan 1997; Sengor et al. 1988). During late Permian, rifting along the northern margins of the Gondwanaland resulted in a Cimmerian micro-continent and accompanied back arc basins in the Paleo-Tethys (Sengor et al. 1988), followed by the opening of the Neo-Tethys (Van der Voo et al. 1999; Patriat and Achache 1984). According to Garzanti (1993), seafloor spreading started in the Indian Ocean during the Valanginian and was subsequently followed by subduction of Neo-Tethys oceanic crust in middle to late Cretaceous. The Indian plate underwent an unusual sudden acceleration during its northward journey from late Cretaceous (67 Ma) to early Eocene (50 Ma), about 20 cm/year, and then dramatically slowed to 5 cm/year during its collision with Asia (Lee and Lawver 1995; Patriat and Achache 1984; McKenzie and Sclater 1971). The recognition of two subduction zones within the Neo-Tethys suggests that India first collided with the Kohistan-Ladakh Arc at the Makran-Indus Trench at ca. 65–61 Ma and then with Asia along the Shyok-Tsangpo Trench at ca. 50 Ma (Burg 2011; Chatterjee and Scotese 2010; Khan et al. 2009; Ali and Aitchison 2008; Van der Voo et al. 1999; Reuber 1986). Chatterjee (2013) summarized the whole tectonic play (i.e., sequential rifting of the Indian plate from Gondwanaland and its subsequent collisions with the Kohistan-Ladakh Arc and Asia) into nine major tectonic evolutionary stages. These include (i) separation of east Gondwanaland from west Gondwanaland (~170 Ma); (ii) separation of India from Antarctica-Australia (~130 Ma); (iii) separation of Madagascar from India (~90 Ma); (iv) collision of India with Kohistan-Ladakh Arc (~88 Ma); (v) separation of Laxmi Ridge from India (~70 Ma); (vi) separation of Seychelles from India (~65 Ma); (vii) acceleration of Indian plate as an island continent (~65–52 Ma); (viii) initial collision of India with Asia (~50 Ma); and (ix) indentation, rotational underthrusting, and oroclinal bending of the Indian plate, i.e., in relation to the Himalayan orogeny (~10 Ma).

The study area forms the southern extremity of the Hazara Basin, which is part of Himalayan foreland fold and thrust belt (Fig. 1). This resulted from continent-continent collision between Indian and Eurasian plates during Ypresian times (Rowley 1996; Coward et al. 1988; Yeats and Hussain 1987; Calkins et al. 1975). The area is highly deformed and the rock exposures represent Indian plate sedimentary stack from north of the Main Boundary Thrust (MBT) to the south of Panjal Fault (PF). A north-south compressional regime is depicted by the presence of east-west trending major structures (e.g., MBT and PF) and other local faults in the study area and its surroundings (Fig. 1). The study area is situated in the footwall of Nathia Gali Thrust (NGT) in the southwest portion of the Hazara Basin, being part of the western Hazara Range (Coward et al. 1988; Fig. 1). Structurally, the area is highly deformed due to the Himalayan orogeny (Fig. 1). A number of thrust faults branching from the main Haro Fault are present in the area. These include Kohala Fault, Palaka Fault, Bahamala Fault, Koimera Fault, Koinara Fault, and Hazara/NGT (Fig. 1).

During the Mesozoic, the Hazara Basin was an important depocenter at the northern margin of the Neo-Tethys, where thick sediment accumulation occurred (Chaudhry et al. 1998; Shah 1977). Afterward, thick shallow water carbonate platform deposits (oolitic-pelletoidal shoals) from Toarcian to Callovian Samana Suk Formation deposited in the Hazara Basin (Chaudhry et al. 1998; Shah 1977). A restricted environment prevailed after the deposition of Samana Suk Formation and resulted into the deposition of mid-outer shelf Chichali Formation (consisting of condensed, pyrite-rich, and belemnite black siltstone) elsewhere in the Hazara Basin, whereas the Samana Suk Formation exhibited an unconformable contact with the Chichali Formation elsewhere in the Hazara Basin. In the Upper Cretaceous (Cenomanian), rapid northward drift of the Indian plate from Madagascar resulted in deepening of the Hazara Basin and subsequent deposition of the Kawagarh Formation (Ahsan and Chaudhry 2008). Later on, collision between India and the Kohistan Island Arc resulted in a sea-level regression during the Upper Eocene, and hence, a marginal marine and evaporitic

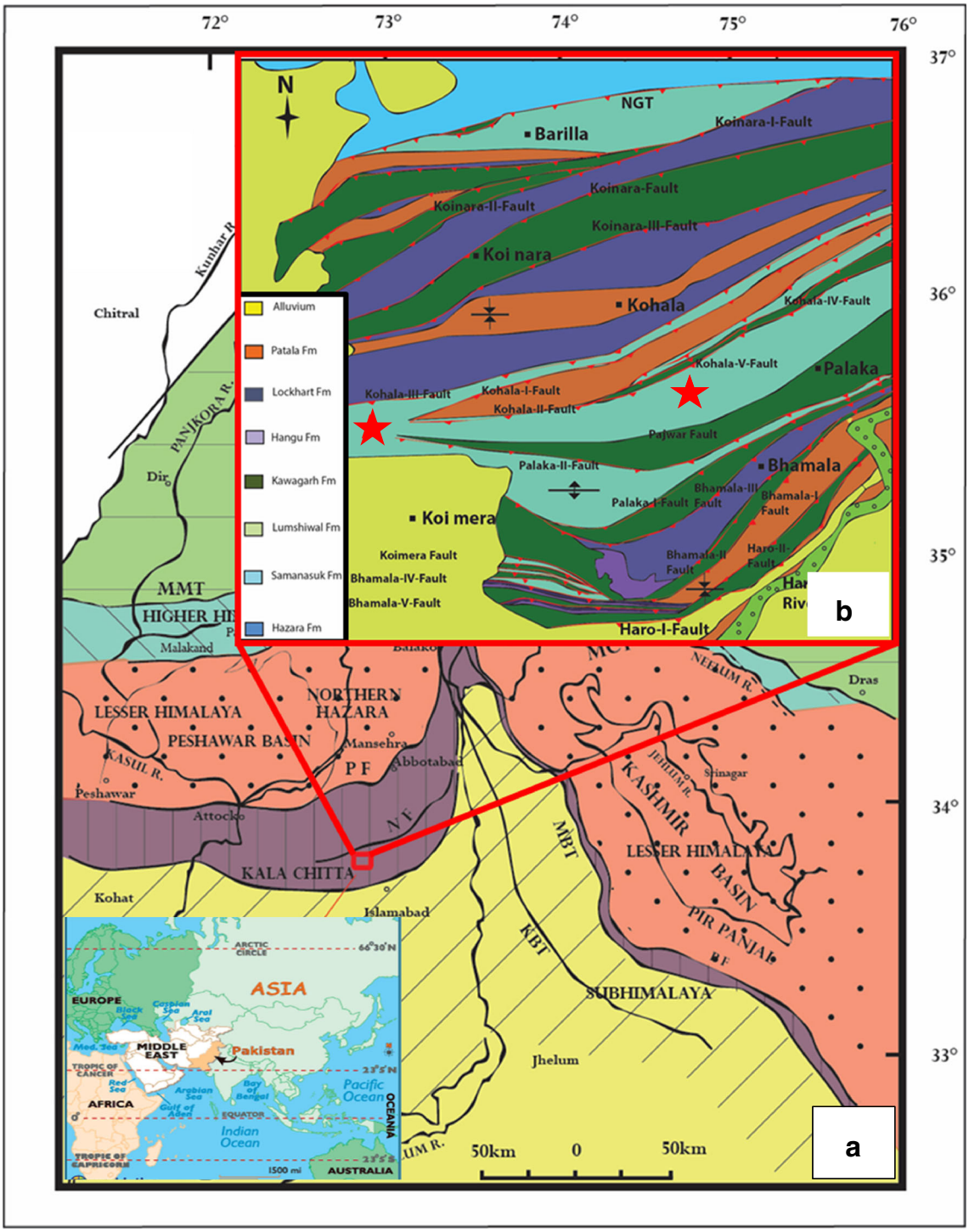

Fig. 1 a Geological map of the NW Himalayan fold and thrust belt. **b** Inset shows the location map of the study area and studied sites (*red stars*). Note that Nathiagali Fault (NF) is represented as Nathaigali Thrust (NGT) in the inset map

environment prevailed in the Hazara Basin, resulting in the deposition of early to middle Eocene Kuldana Formation (shales, marls, and gypsiferous layers) and subsequent deposition of the Murree Formation. In Fig. 2, a simplified stratigraphic column is shown illustrating the stratigraphy of the southern Hazara Basin.

Methodology

Extensive outcrops of the Samana Suk Formation are exposed in the Khanpur area (i.e., along Taxila-Haripur road). Detailed field investigations of the carbonate succession in the study area were carried out. Systematic as well as random sampling

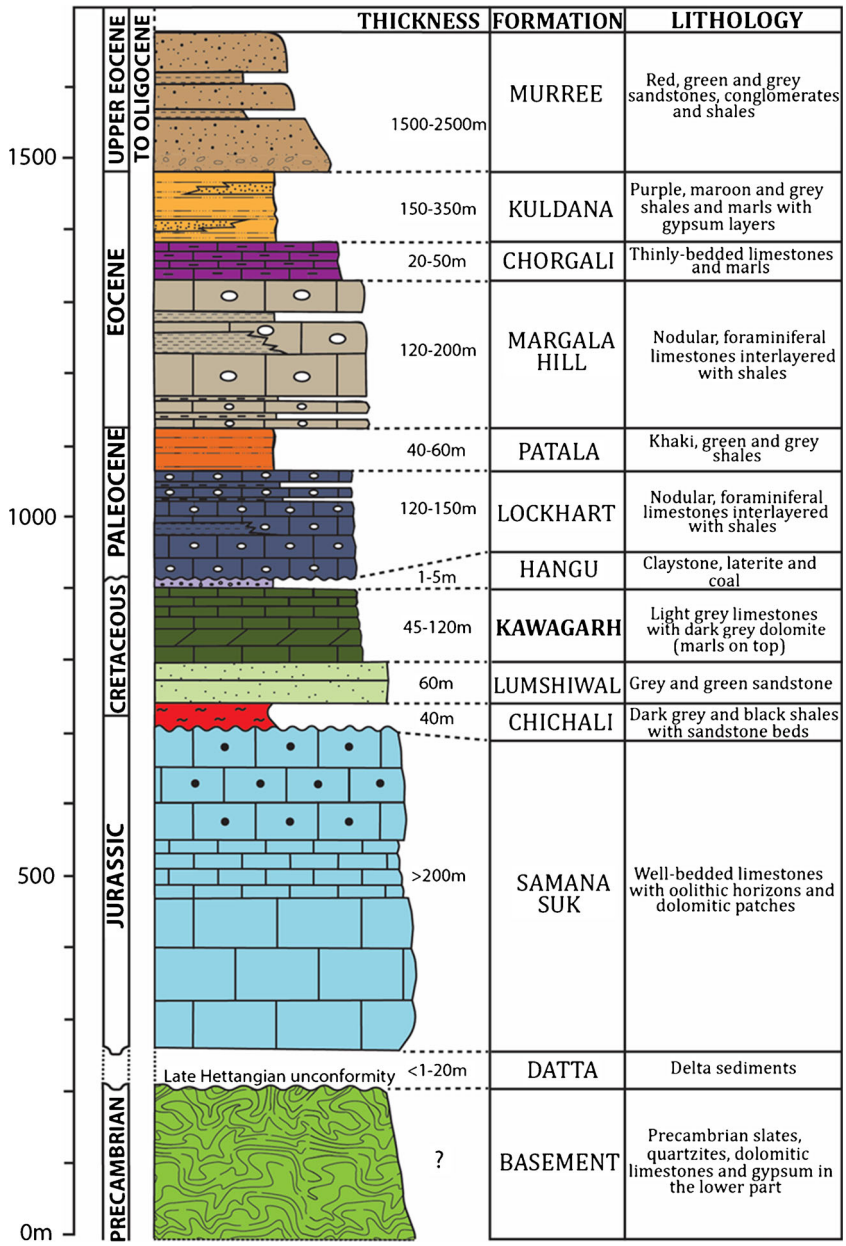

Fig. 2 Stratigraphic column of the southern Hazara Basin

of various calcite and dolomite phases was done. Multiple sections were studied and sampled so as to cover the whole stratigraphic interval as good as possible. Sampling density is mainly governed by observed features. In total, 139 collected samples represent the limestone, various dolomite phases, and calcite cement. Dolomite and limestone are easily differentiated on the basis of clear color contrast at the outcrop. The rock samples were cut and polished and then stained with Alizarine Red S and K-ferricyanide solution (Dickson 1966). Different dolomite phases, calcite phases, and the original limestone are distinguished based of stained samples.

Eighty-four thin sections were prepared at the Hydrocarbon Development Institute of Pakistan (Islamabad) and studied for petrographic observations using conventional microscopy (Olympus CX31 along with DP-21 camera attachment). Cathodoluminescence microscopy was performed in the Institute of Geology, Jagiellonian University, Krakow (Poland), using an optical microscope cathodoluminescence stage (CL8100 MK5) with operating conditions of 12–17-kV gun potential, 350–600-μA beam current, and 0.05-Torr vacuum.

Bulk mineralogy, percentage composition, and dolomite stoichiometry of the selected samples were resolved by carrying out X-ray diffraction (XRD) analyses of selected 18 powdered samples using PANalytical X'Pert PRO X-ray diffractometer (Cu-Kα radiation ~45 kV, 40 mA). The scan speed was set at 0.2°θ min^{-1} and sampling interval at 0.001°θ per step. The dolomite stoichiometry was calculated by using Lumsden's equation (1979) to the measured d_{104} spacing

(M = 333.3 × d spacing − 911.99) and expressed as mol% $CaCO_3$. Stable oxygen and carbon isotope analyses ($\delta^{18}O$ and $\delta^{13}C$) of 37 selected samples of different dolomite, calcite cements, and host limestone were carried out in the Isotope Application Division, Pakistan Institute of Nuclear Science and Technology, Islamabad (Table 1). All stable isotope values are reported in per mill (‰) relative to Vienna Pee Dee Belemnite (V-PDB) by assigning a $\delta^{13}C$ value of +1.95‰ and a $\delta^{18}O$ value of −2.20‰ to NBS19. The carbonate powders were reacted with 100 % phosphoric acid (density >1.9; Wachter and Hayes 1985) at 75 °C in an online carbonate preparation line (Carbo-Kiel—single-sample acid bath)

Table 1 Table showing part of the database used in the present studies

Serial no.	Section name	Sample no.	Rock type	$\delta^{18}O$‰ (V-PDB)	$\delta^{13}C$‰ (V-PDB)	Ca stoichiometry	Porosity (%)	Permeability (mD)
1	Duhamaka	DM-1	LS	−4.1	1.2			
2		DM-3	WC-I	−12.94	0.6			
3		DM-4	Dol. II	−9.76	1.21			
4		DM-5	Dol. II	−6.48	1.77	49.5		
5		DM-6	Dol. II	−8.81	0.95	50.8	3.24	0.05
6		DM-7	Dol. II	−9.15	1.23			
7		DM-8 A	LS	−5.2	0.78			
8		DM-9	Dol. I	−4.86	0.98	49.2		
9		DM-10	Dol. I	−4.51	1.05			
10		DM-11	Dol. I	−5.12	1.1			
11		DM-12	Dol. II	−6.17	2.14		3.57	0.08
12		DM-13	WC-I	−13.59	1.4			
13		DM-14	LS	−4.8	0.5			
14		DM-16	SD	−12.17	1.2	49.2		
15		DM-17	Dol. II	−7.23	2.07	50.2	3.52	0.09
16		DM-18	Dol. II	−9.54	2.05			
17		DM-21	Dol. I			50.2	10.33	1.36
18		DM-23	Dol. II	−8.95	2.24	50.4		
19		DM-29	Dol. II	−9.12	2.31			
20	Khui Mera	KM-3	Dol. I	−5.84	2.37			
21		KM-7	Dol. II	−10.18	1.77			
22		KM-9	Dol. II	−8.45	1.04			
23	Suraj Gali	SG-2	SD	−12.43	1.45	49.8	4.41	4.17
24		SG-5	Dol. II			50.5	3.14	0.58
25		SG-10	Dol. II	−10.12	1.69		3.77	1.21
26	Kharala	KR-1	Dol. I	−5.72	1.77			
27		KR-4	Dol. I			49.2	5.41	8.97
28		KR-6	TC	−4.42	−2.18			
29		KR-8	Dol. I				5.63	5.18
30	Bestway	BW-2	Dol. I	−3.93	1.98	49.9	5.68	4.86
31		BW-4	Dol. II	−7.12	1.5			
32		BW-7	Dol. II	−6.85	1.45	51.5		
33		BW-8	Dol. II	−6.18	1.27	51.3	4.56	1.15
34		BW-10	Dol. I	−3.91	0.95	50.1	3.47	7.56
35		BW-11	Dol. I	−3.96	1.65			
36		BW-13	Dol. I	−4.24	1.1	49.2		
37		BW-14	WC-II	−8.56	0.72			
38		BW-18	Dol. II	−6.14	−0.4	50.5		
39		BW-21	Dol. II	−7.21	1.09	51.1		
40		BW-22	WC-II	−6.94	1.1			
41		BW-24	Dol. II	−6.52	1.25	50.7		

connected to a Finnigan MAT 252 mass spectrometer. Dolomite isotopic composition values are corrected by fractionation factors given by Rosenbaum and Sheppard (1986). Back-scattered electron microscopy along with energy-dispersive X-ray spectrometry was carried out in the Geosciences Advance Research Lab, Islamabad (Geological Survey of Pakistan).

To determine the petrophysical properties, standard helium porosity and Klinkenberg permeability measurements were performed in the Geology and Reservoir (G&R) Labs of Oil and Gas Development Company Limited (OGDCL), where 12 samples representing various facies were measured from plugs (~5 cm in length and ~3 cm in diameter) using standard porosity-permeability measuring instrumentation (core-measuring sampler-100) under net pressure of 1000 psi.

Results

Field observations

Field investigations revealed interbedded limestone and dolomite in the studied sections. The thickness of the host limestone and dolomite is variable in different sections, which ranges from a few meters to tens of meters (Fig. 3a). The host limestone is clearly differentiable from the dolomite as it gives off-white color in contrast to dark grey colored dolomite (Fig. 3a, b). Sharp contact between the off-white colored limestone and the dark grey colored dolomite is observed (Fig. 3b, c). Limestone shows thin to medium bedding near the contact with the dolomite, whereas dolomite mostly destroys primary sedimentary features (e.g., bedding planes). In the study area, two distinct types of matrix dolomite are recognized on the basis of color contrast. These include (i) dark grey colored dolomite (Dol. I) and (ii) light grey colored dolomite (Dol. II; Fig. 3d, e). The latter locally occur next to each other. Furthermore, pore-filling, coarse to very coarse crystalline calcite mostly occurs in Dol. I. It is notable that white calcite (WC) post-dates matrix, dark grey colored dolomite (Dol. I; Fig. 3f). In addition to two phases of matrix dolomite, yellowish-white colored dolomite cement phase (saddle dolomite (SD)) mostly occur as veins and vug fillings in the matrix dolomite (Fig. 4a–d). This dolomite cement mostly occurs in the pore spaces of dark grey colored dolomite (Dol. I; Fig. 4a, b). In addition, vug-filling dolomite cement (SD) also occurs in light grey colored dolomite (Dol. II; Fig. 4c). On the basis of surface texture, it is noteworthy that dark grey colored, replacive matrix dolomite (Dol. I) exhibited coarse crystalline affinity as compared to light grey colored dolomite (Dol. II; Fig. 4).

The average thickness of majority of dolomite cement (SD) veins is 3 cm, although veins as thick as 10 cm are also observed (Fig. 4e). It is observed that vein-filling dolomite cement mostly originated from vug-filled dolomite cement, since these dolomite pockets are the main source from which majority of white dolomite veins radiate, diverge/spread, and follow existing fracture pattern (Fig. 4d, e). Cross-cutting relationship and pore fillings within the white dolomite, which gives brownish appearance on weathered surface, indicate that late stage, white calcite post-dates white dolomite cement (Fig. 4d, e).

In addition to the above mentioned diagenetic phases, other distinct features observed in the study area include brecciation, dolomite-filled burrows, and stylolites (Figs. 3d, g and 4d).

Petrography and mineralogy

Petrographic observations

Microscopic examination of precursor limestone, various dolomite, and calcite phases were performed to establish a detailed paragenetic sequence of various diagenetic phases in relation to field observations. In order to achieve this objective, conventional, cathodoluminescence, and back-scattered electron microscopy was carried out on the selected thin sections. Dolomite phases are differentiated on the basis of shape and size of crystals using the classification scheme of Sibley and Gregg (1987).

The studied sections display oolitic limestone, medium to coarse crystalline dolomite (Dol. I), fine to medium crystalline dolomite (Dol. II), pore-filling, coarse crystalline SD cement, first phase of white calcite (WC-I), second phase of white calcite (WC-II), and transparent calcite (TC), respectively. Moreover, other diagenetic alterations that include dedolomitization, brecciation, and stylolites are also observed in the studied rocks.

i. Limestone

The studied oolitic limestone texture ranges from wackestone to grainstone. It is evident that initial phase of calcite cement (Cal. I) mostly bordered oolitic grains (Fig. 5a). The oolitic limestone is intensely fractured and contained calcite cement (Cal. II) that post-date dolomite cements (Dol. I?; Fig. 5a). Bedding-parallel stylolites are observed in the studied limestones.

ii. Replacive dolomite

Dolomitization process mostly obliterated the primary sedimentary structures of the host limestone but rarely preserved oolitic structures (Fig. 5b). The sharp contact between the host limestone and the dolomite observed in the outcrop is found also at the thin section scale (Fig. 5c).

Medium to coarse crystalline, planar dolomite (Dol. I)

Euhedral to subhedral, medium to coarse crystalline, and planar dolomite (Dol. I) forms the first phase of

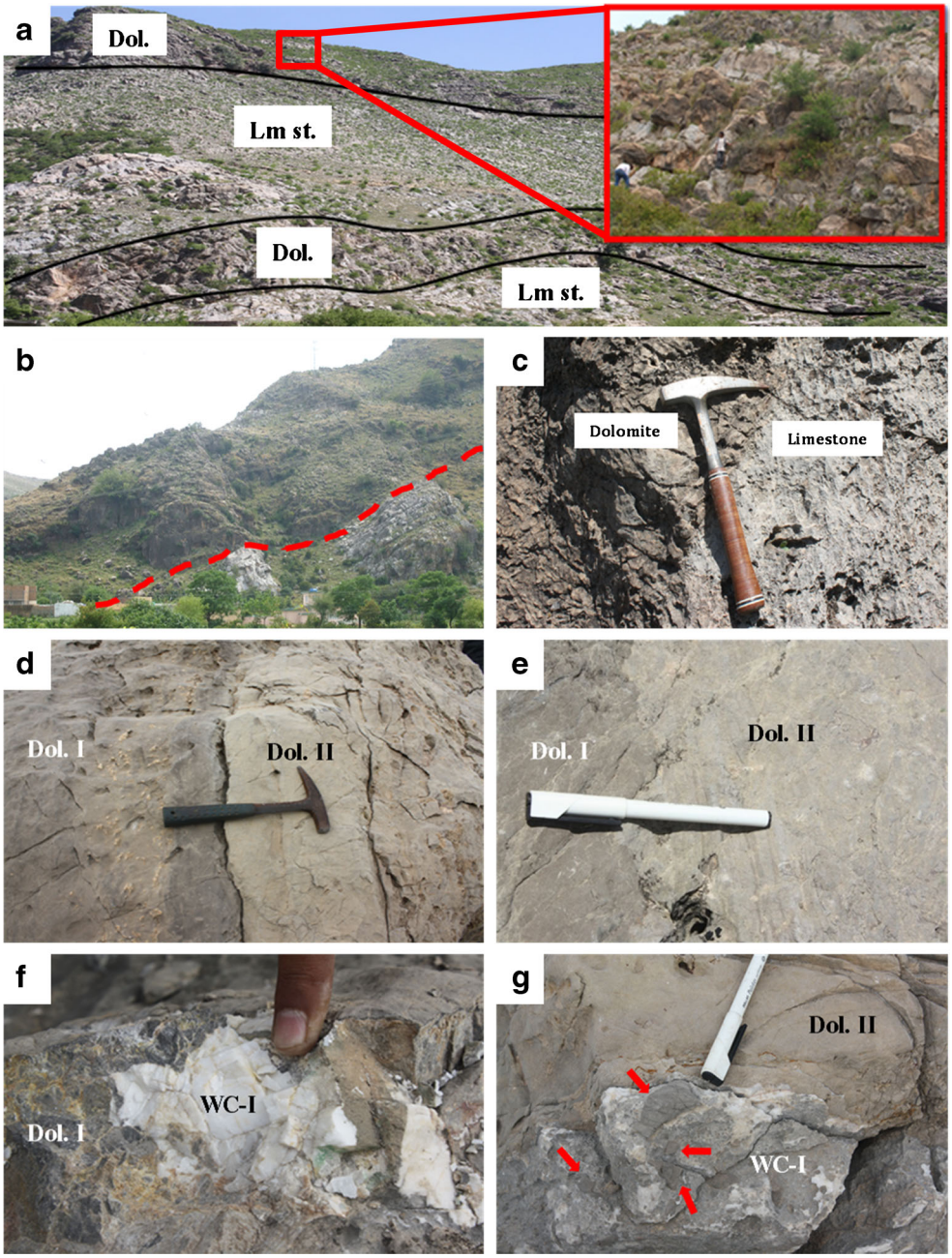

Fig. 3 Field observations showing the distribution of dolomite geo-bodies. **a** Panoramic view of bedding-parallel dolomite bodies in the study area. Inset shows the close-up view of interbedded dark grey colored dolomite and off-white colored limestone. **b**, **c** Sharp contact between dark grey colored dolomite and white colored limestone. **d**, **e** Sharp contact between dark grey colored dolomite (Dol. I) and light grey colored dolomite (Dol. II). **f** Pore-filling white calcite (WC-I) in dark grey colored dolomite (Dol. I). **g** In light grey colored dolomite (Dol. II), fracture-filled white calcite (WC-I) cementing dark grey colored dolomite (Dol. I) brecciated clasts

dolomitization (Fig. 5a, b). Such replacive phase was initiated from the fractures in the host limestone, followed by complete replacement (Fig. 5a, b). In addition, sharp contact between the host limestone and Dol. I is observed (Fig. 5c). Dol. I also show sharp contact with the second phase of dolomitization (Fig. 5d) and exhibited cloudy cores surrounded by clear cemented rims (Fig. 5e, g). Intercrystalline pore spaces and fractures are mostly filled by white calcite (Fig. 5f, g), whereas late stage vugs are mostly occluded by coarse crystalline, nonplanar dolomite termed as saddle type (SD; Fig. 5e). Selective dedolomitization of Dol. I emerged from the interaction of initial phase of calcite with the Dol. I, which resulted in the partial alteration of bordered dolomite as observed in Fig. 5g, whereas the core remained unchanged (Fig. 6g, h). In addition, initial corrosion may have led to the complete dissolution of the pre-existing dolomite crystals, which may contribute toward the porosity enhancement of these dolomite bodies (Fig. 6g). Late stage percolation of calcite-rich fluids resulted in the brecciation and cataclastic deformation of Dol. I (Fig. 5h).

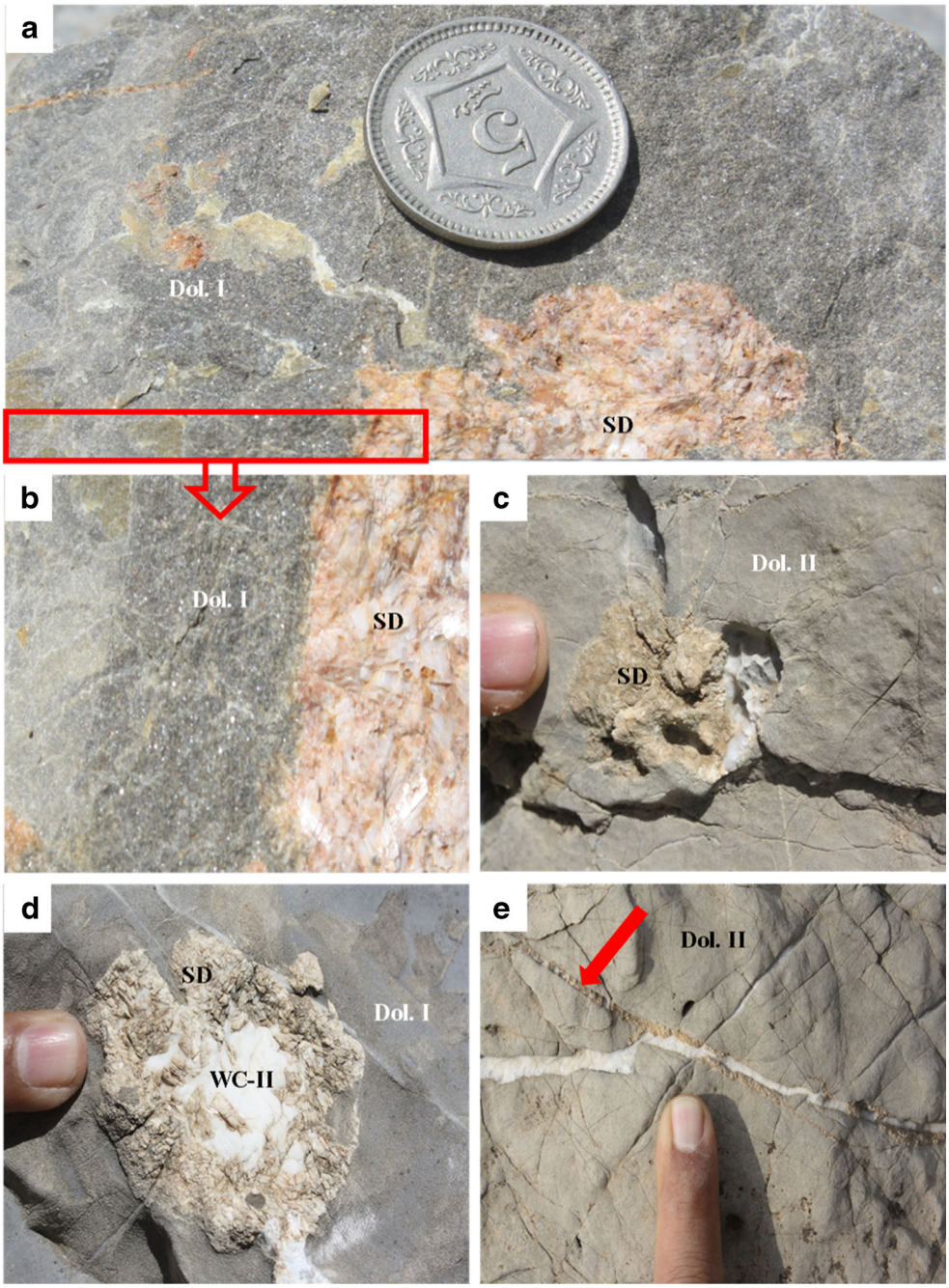

Fig. 4 Field observations of dolomite bodies. **a**, **b** Pore-filling yellowish white colored dolomite cement (SD) in dark grey colored dolomite (Dol. I). Close-up view of the pore-filling dolomite cement in dark grey colored dolomite (Dol. I). **c** Vug fillings of brownish weathered colored saddle dolomite (SD) in light grey colored dolomite (Dol. II). **d** Large vug partially cemented by saddle dolomite and then filled by white calcite (WC-II) post-dates already filled dolomite cement (SD) in matrix dolomite (Dol. I). **e** White calcite (WC) vein post-dates fracture-filled dolomite cement (*red arrow*) vein in matrix dolomite (Dol. II)

Fine to medium crystalline, planar to nonplanar dolomite (Dol. II)

Pervasive planar to nonplanar dolomite (Dol. II) displays sharp contact with the initial phase dolomite (Dol. I; Fig. 5d). This dolomite phase shows marked textural difference (i.e., fine crystalline and nonplanar) from the initial phase of dolomite Dol. I (Fig. 5d). This replacive dolomite phase (Dol. II) occurred before the initial stage of calcite emplacement as calcite mostly occurs as veins and fracture fillings in Dol. II (Fig. 3g). In addition, both replacive dolomite phases pre-date calcite cement phases (Fig. 6a). Pore-filling SD cement is mostly in contact with Dol. I and Dol. II (Fig. 6f).

i. Dolomite cement

Pale-yellow coarse crystalline SD

Milky white to pale-yellow coarse to very coarse crystalline, curve-shaped dolomite (SD) mostly occurs as pore-filling cement in the earlier discussed dolomite phases (i.e., Dol. I and Dol. II; Fig. 4a, b, d). Where vuggy porosity was present

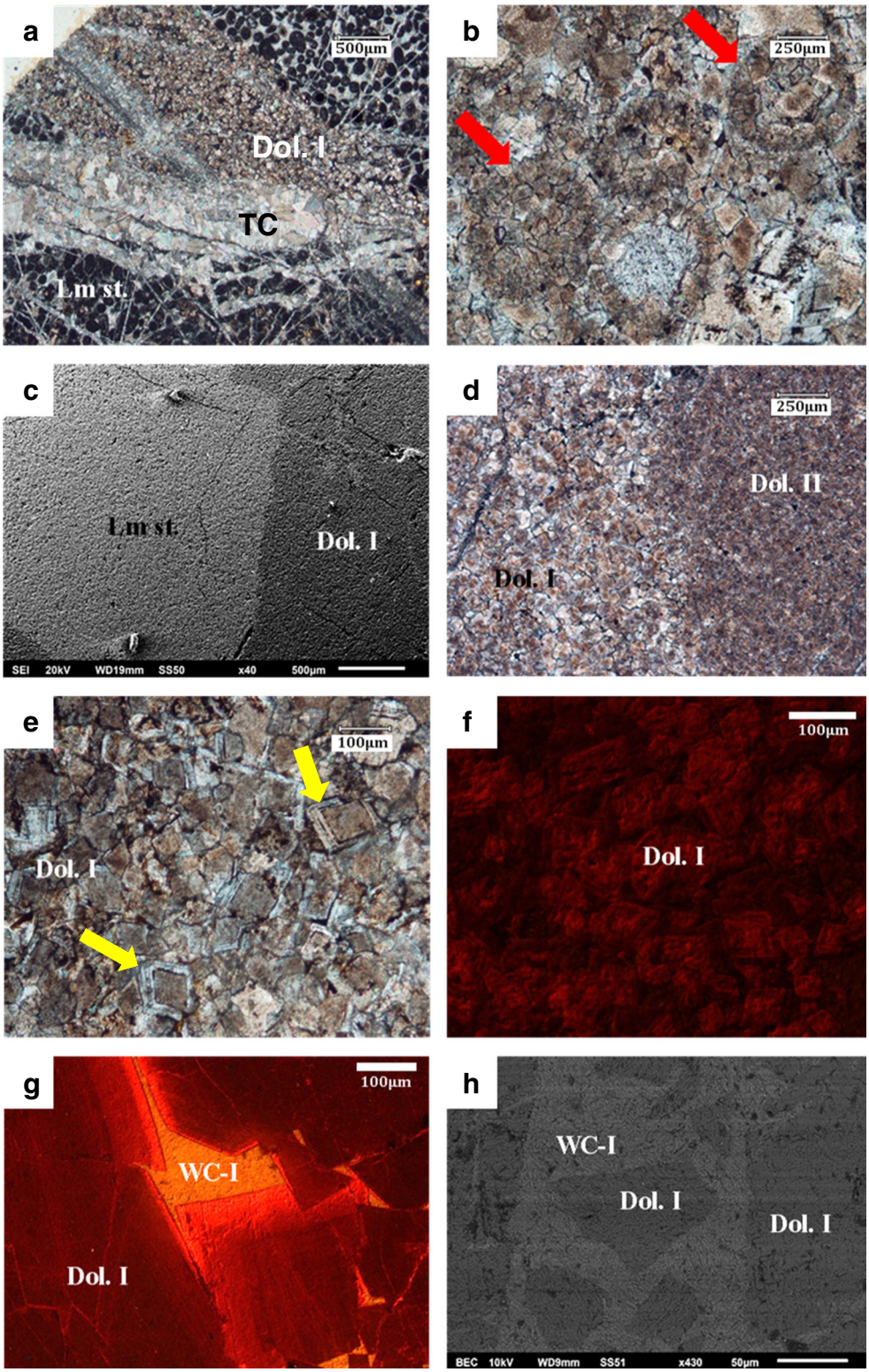

Fig. 5 Photomicrographs showing the petrographic description of studied limestone and dolomite. **a** Initial phase of matrix dolomite pre-dates late stage calcite cementation in oolitic limestone. **b** Inherited oolites preserved in the dolomitized limestone. **c** Back-scattered electron microscopic observations show clear contrast between dark grey colored dolomite and light grey colored limestone. **d** Coarse crystalline dolomite (Dol. I) exhibiting sharp contact with fine crystalline dolomite (Dol. II). **e** Coarse crystalline, planar dolomite (Dol. I), note that borders are partly calcitized (*yellow arrow*). **f**, **g** Cathodoluminescence petrography showing calcite fillings in intercrystalline pore spaces of coarse crystalline dolomite (Dol. I) whereas close-up view of the intercrystalline calcite cement. **h** Back-scattered electron microscopic studies showing dolomite clasts (Dol. I) in white calcite (WC)

in the matrix dolomite (Dol. I and Dol. II), saddle dolomite crystals largely occupy these open spaces (Figs. 4c, d and 6e, f). Where the dolomite is in contact with calcite, it commonly consists of corroded boundaries of dolomite crystals (Fig. 6g). The outlines of these dolomite crystals are not always well defined due the partial replacement or assimilation by WC-I.

Some centimeter-sized elongate irregular "curve-shaped" pale-yellow dolomite crystals (CSD) are in contact with

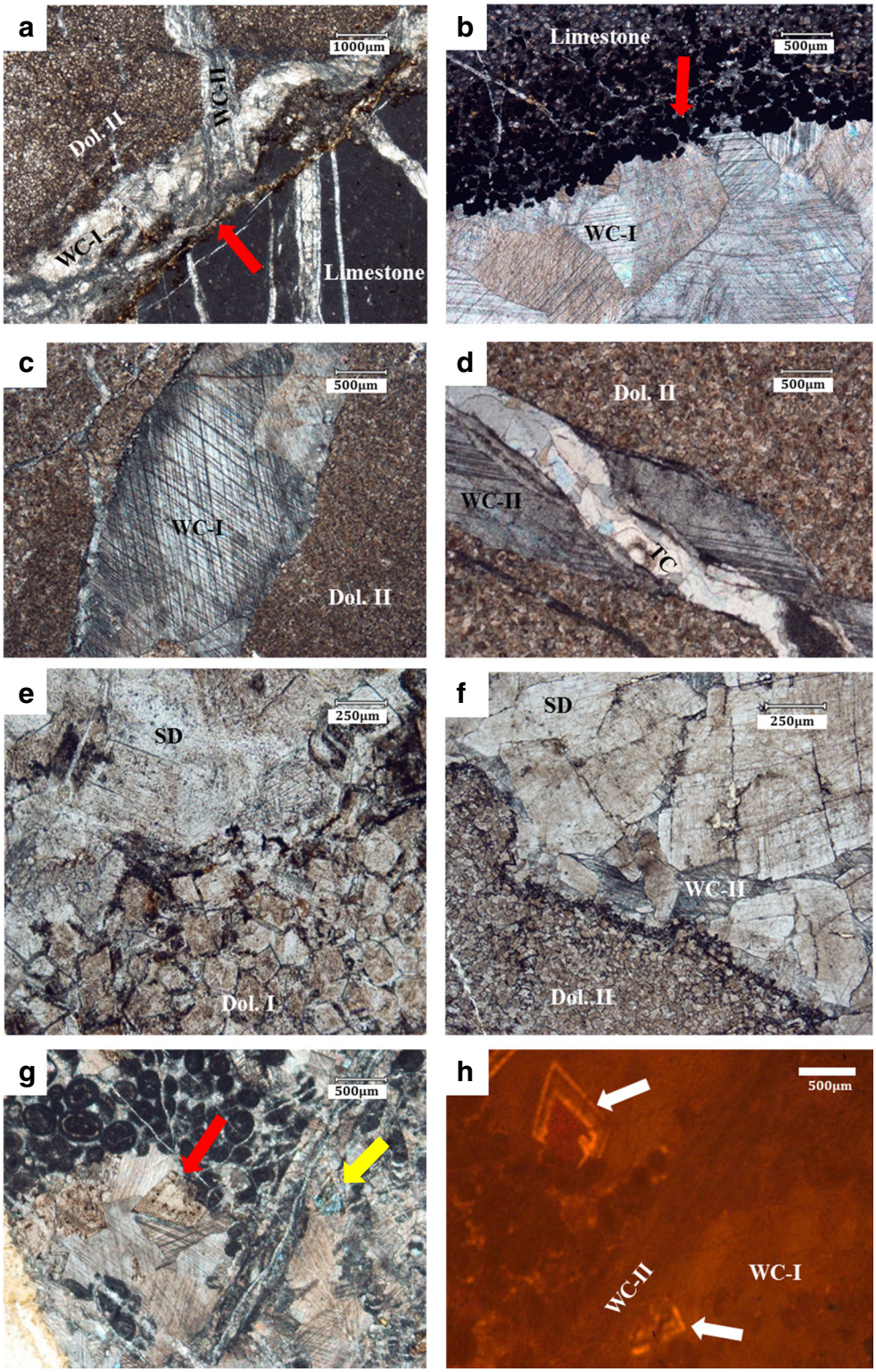

Fig. 6 Petrographic observations of the dolomite rocks. **a** Limestone-dolomite sharp contact, whereas late calcite cements (WC-I and WC-II) post-date early dolomite cement. *Red arrow* shows stylolite post-dating calcite cements. **b** Dodecahedral grains of pyrite (*red arrow*) pushed apart by white calcite (WC-I). **c**, **d** White calcite (WC-I) post-dating dolomite cement (Dol. II). Late stage telogenetic calcite (TC) marks the last diagenetic event of the paragenetic history. **e** Irregular contact between coarse crystalline dolomite (Dol. I) and coarse crystalline dolomite (SD). **f** Sharp contact between fine crystalline dolomite (Dol. II) and coarse crystalline dolomite cement (SD). Furthermore, white calcite (WC-II) filled intercrystalline pore spaces in SD. **g**, **h** Plane polarized (PPL) and CL photomicrograph showing calcitized dolomite (*white and red arrows*) in WC-I, whereas late stage calcite (WC-II) post-dates these early phases. Dissolution porosity is evident as dolomite crystals dissolved out (*yellow arrow*)

replacive coarse crystalline dolomite (Dol. I) and fine to medium crystalline dolomite (Dol. II; Fig. 6c, d). Such very coarse crystalline dolomite consists of planar to nonplanar, coarse crystalline dolomite that shows undulose extension characteristic of saddle dolomite (Fig. 6e; Radke and Mathis 1980; Searl 1989). These crystals developed here symmetrically along the openings within the matrix dolomite Dol. I and Dol. II. The long axes of these crystals are commonly perpendicular to the wall with the matrix dolomite, but at contacts between the coarse crystalline dolomite and the matrix

dolomite, they form curvilinear semi-spherical or rosette-like aggregates (Fig. 4c, d). The curve-shaped outline in two dimensions may relate to the saddle-like nature of these crystals (Fig. 6f). Commonly, the curve-shaped crystals are composite and grade into massive coarse crystalline dolomite SD (Fig. 6f). Bedding-parallel stylolites cross-cut the curve-shaped dolomite, outlining the contacts between the different dolomite types. From the description above, it is clear that the SD locally appears as a cement product.

ii. Calcite phases

Three phases of calcite cement are recognized that mostly occur as pore filling and associated with faults, fractures, and vugs. Out of these three calcite phases, two distinct calcite phases are differentiated on the basis of cleavage or deformational twining characteristics that include (i) multidirectional cleavage-twinned calcite (WC-I) and (ii) unidirectional cleavage-twinned calcite (WC-II; Fig. 6c, d). Various authors contributed toward the understanding of paleostress estimation using cleavage-twinned calcite (Lacombe 2010; Lacombe et al. 2007; Ferrill et al. 2004; Gonzales-Casado and Garcia-Cuevas 1999). In the present studies, above mentioned technique helped in discerning two distinct calcite phases (WC-I and WC-II). Multidirectional twinned calcite (WC-I) mostly pre-dates unidirectional twinned calcite (WC-II; Fig. 6a, h).

First phase of calcite cementation (i.e., WC-I) chiefly occludes intercrystalline pore spaces within the Dol. I (Fig. 5f, g). Subsequently, dedolomitization of the outer rimmed dolomite is more frequent as compared to the core of the dolomite crystals (Fig. 6h). In addition, brecciated clasts of Dol. I in the WC-I indicate late stage origin (Fig. 5h). It is observed that dodecahedral crystals of pyrite up to 2 mm in diameter occurred along the margins of pore-filled calcite (WC-I; Fig. 6b). The second phase of calcite cement (WC-II) largely occurs as pore fillings in SD, whereas matrix dolomites (Dol. I and II) also contain such calcite as veins and fracture fillings (Fig. 6d, f). Based on cross-cutting relationship, WC-II post-dates WC-I and matrix dolomite (Fig. 6h). Furthermore, late stage TC post-date all the calcite and dolomite phases (Fig. 6d).

Mineralogical studies

Back-scattered electron microscopy (BSEM) in conjunction with energy-dispersive X-ray spectrometry (EDX) helped in differentiating calcite, dolomite, and other diagenetic minerals (Fig. 7a). As discussed in the earlier section, limestone, dolomite, and calcite are differentiated on the basis of color contrast. Furthermore, EDX studies revealed that light grey color represents calcite engulfing dark grey colored brecciated dolomite clasts (Fig. 7b). In addition, Fe-bearing dodecahedral minerals (possibly pyrite) are associated with initial stage of calcite WC-I (Fig. 7c).

Dolomite stoichiometry

According to Reeder (1991), the crystal lattice of an ideal dolomite is composed of alternating layers of Ca and Mg, separated by layers of carbonate ions that represented stoichiometrically as $Ca\,Mg(CO_3)_2$. Powdered dolomite samples were analyzed for X-ray diffraction studies in order to determine the stoichiometry of the dolomite. The composition of the analyzed samples of dolomite mostly ranges between 75 and 100 % dolomite, and the Ca content varied between 49.2 to 51.5 mol% $CaCO_3$ (Table 1).

Isotope geochemistry

Stable isotope analyses

A total of 37 samples were selected for stable isotope analyses ($\delta^{18}O$ and $\delta^{13}C$) from various studied sections (Table 1). Selected samples include limestone and various diagenetic phases of calcite and dolomite described in the preceding section. In order to correlate the stable isotope results of the study area with known seawater isotopic signatures of the middle Jurassic carbonates in the region, stable isotopic signatures of the brachiopod and belemnite samples analyzed from Kachch mainland (western India) were reported. These show that isotopic signatures of carbonates precipitating from Callovian-Bajocian seawater range from −2.8 to −1.8‰ $\delta^{18}O$ V-PDB and +0.0 to +1.8‰ $\delta^{13}C$ V-PDB, respectively (Fürsich et al. 2004). Stable isotope signatures of the host limestone show depleted $\delta^{18}O$ values (−5.2 to −4.8‰ V-PDB), whereas $\delta^{13}C$ values ranging from +0.5 to +1.2‰ V-PDB (Fig. 8). Such depleted $\delta^{18}O$ values indicate that the host limestone is effected by diagenetic fluids and/or affected by higher temperatures as compared to the ambient temperature of the host rock.

Various diagenetic phases (i.e., replacive dolomite, cement dolomite, white calcite cement, and transparent calcite) possess distinct isotopic signatures, which reflect to their origin in relation to different diagenetic conditions. First phase of dolomitization (Dol. I) shows a less depleted oxygen isotopic signatures (−5.84 to −3.91‰ V-PDB), whereas carbon isotopic values (+0.6 to +2.37‰ V-PDB) are within the limit of the carbonate marine seawater signatures (Fig. 8). Second phase of dolomitization (Dol. II) exhibited depleted oxygen values (−10.18 to −6.14‰ V-PDB) and slightly depleted carbon isotopic signatures (−0.4 to +1.77‰ V-PDB), respectively (Fig. 8). In addition, pore-filling, dolomite cement (SD) shows highly depleted oxygen isotope values ranging from −12.17 to −12.43‰ V-PDB, while carbon isotope values are within the limits of marine carbonates (i.e., +1.2 to +1.6‰ V-PDB;

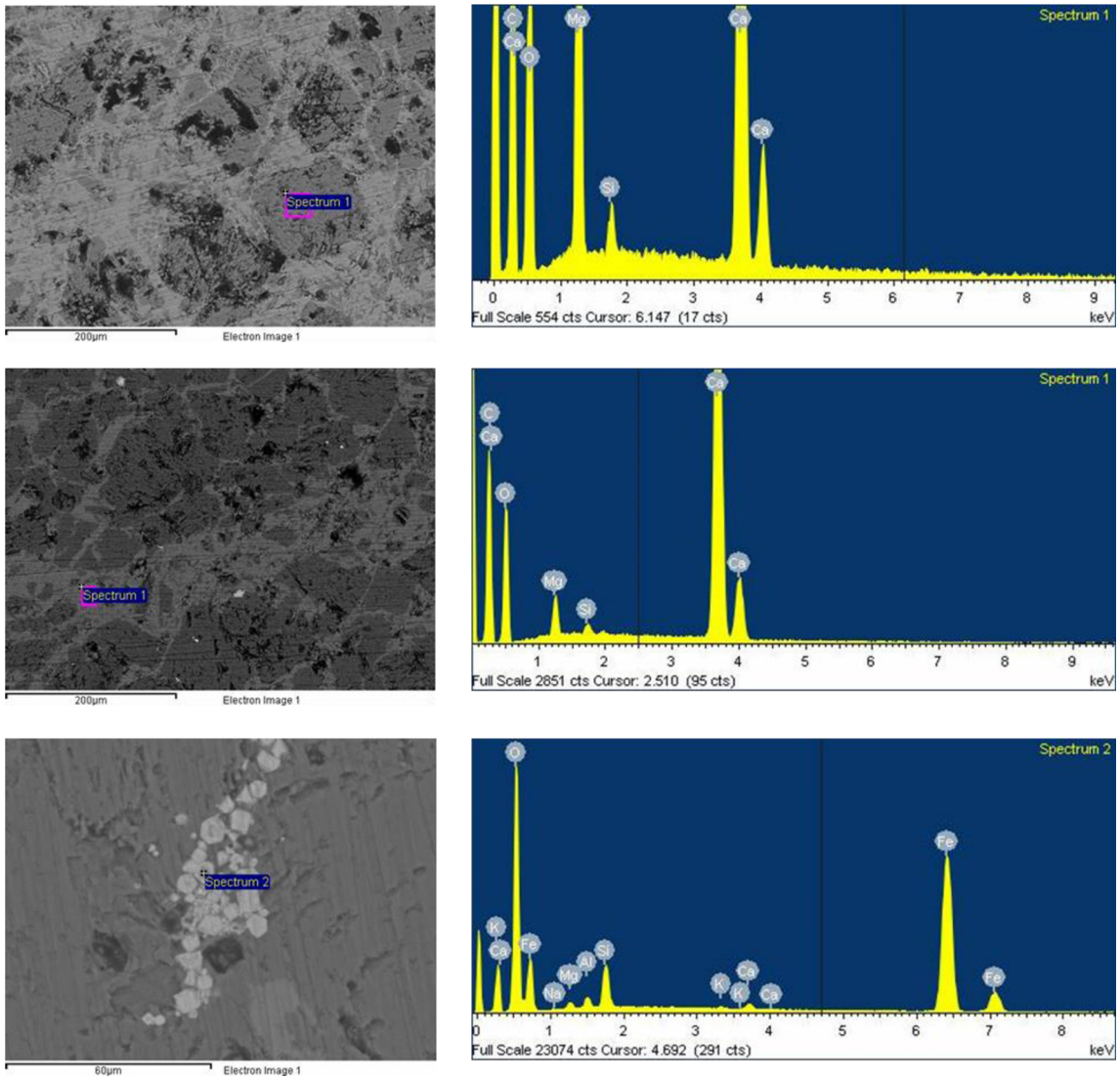

Fig. 7 BSEM and EDX studies of dolomite and calcite phases. **a**, **b** Dark grey colored brecciated dolomite of Dol. I in white calcite (WC-I). EDS studies confirm the elemental composition of the brecciated dolomite and white calcite (WC-I). **c** Pyrite infillings (white colored dodecahedron) in calcite

Fig. 8). Furthermore, first phase of calcite cement (WC-I) displayed even more depleted $\delta^{18}O$ values (i.e., −13.59 to −12.94‰ V-PDB), although $\delta^{13}C$ values (+0.6 to +1.4‰ V-PDB) are within the range of marine carbonate signatures (Fig. 8). The second phase of calcite cement (WC-II) presented relatively less depleted $\delta^{18}O$ values (−8.56 to −6.94‰ V-PDB), whereas $\delta^{13}C$ values range from +0.5 to +1.1‰ V-PDB (Fig. 8). However, last phase of calcite cement (TC) displayed less depleted $\delta^{18}O$ and $\delta^{13}C$ values, respectively (i.e., −4.42 and −2.18), suggesting near-surface meteoric origin.

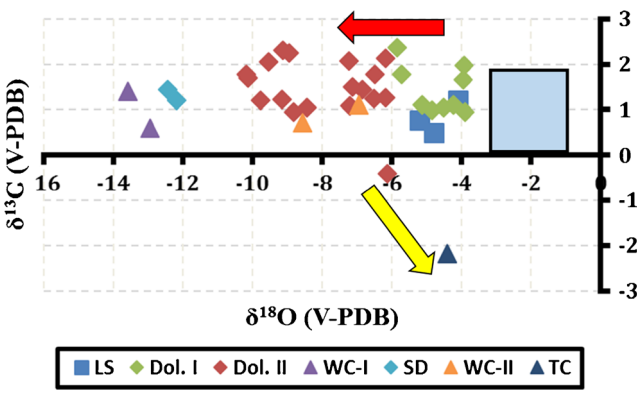

Fig. 8 Detailed paragenetic sequence of the studied dolomite bodies

Reservoir characterization

In order to determine the effect of dolomite development (phases) on petrophysical properties, standard helium porosity and Klinkenberg permeability measurements were performed on the selected plugs representing various diagenetic phases. In the studied carbonate successions, modifications in reservoir

properties resulted from the mineralogical readjustment and mechanical alterations. Dolomitization on the one hand contributed toward porosity enhancement, but occlusion of pore spaces also resulted from dolomite cementation. First phase of dolomite (Dol. I) possesses intercrystalline porosity, which ranges from 5.68 to 10.33 % and permeability ranges up to 8.97 mD (Fig. 9). Brecciation, cataclastic deformation, and dissolution associated with dedolomitization of Dol. I may further enhance the porosity/permeability of such dolomite. The second phase of dolomite (Dol. II) exhibited interlocking pattern/fabrics and contained lesser porosity and permeability values as compared to Dol. I (Fig. 9). Dol. II shows that porosity values vary from 2.25 to 4.56 %, whereas permeability values range from 0.05 to 1.21 mD. As evidenced, fracture intensity is higher in the replacive dolomite as compared to precursor limestone, which also contributes toward porosity enhancement. Anyhow, such fracture distribution is not observed on the plug scale.

Coarse crystalline, pore-filling dolomite (SD) largely occurs as vug-filling cement. Saddle dolomite frequently has occluded the pore spaces in the above mentioned replacive dolomite (i.e., Dol. I and Dol. II) and thus decreased the porosity and permeability (Fig. 9). At the field observation scale, macroscopic pores are specifically filled by SD cement (Fig. 4d). Porosity occlusion related to calcite infilling, where two phases of white calcite (WC-I and WC-II) mostly destroy the pore system. Likewise, late stage transparent calcite further contributes in the porosity reduction of the replacive dolomite (Fig. 9).

Dolomite samples with high porosity but low permeability frequently have cemented veins, although macro-pores are still present. The precipitation of various calcite and dolomite cements has filled the veins and possibly has reduced permeability considerably, whereas most of the matrix pores remained open.

The presence of various diagenetic products has greatly affected the petrophysical properties of the studied carbonates. Replacive dolomitization, brecciation, cataclastic deformation, and dissolution have increased significantly the reservoir properties, whereas dolomite and calcite cementation reduced porosity and permeability of the studied carbonates.

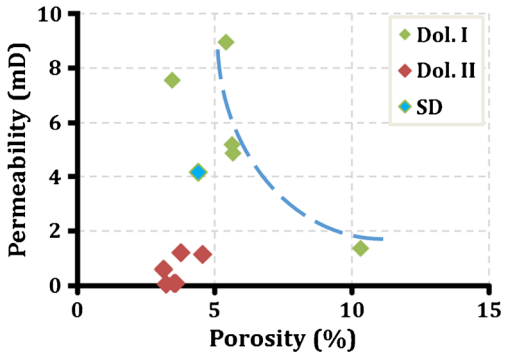

Fig. 9 Stable isotope signatures (O/C) showing depleted oxygen isotope signatures of different dolomite and calcite phases, whereas late stage calcite exhibited depleted carbon signatures. Note that Jurassic marine carbonate signatures are given as *blue box*

Discussion

The study area has experienced multiple episodes of tectonic deformation after the deposition of middle Jurassic carbonate successions. This includes the rifting associated with seafloor spreading during the early Cretaceous, followed by compression-related tectonics due to the subduction of Neo-Tethys oceanic crust during middle to late Cretaceous. Lastly, impact of Indian plate with the Kohistan-Island Arc (i.e., lower Paleocene), and subsequently followed by Indian and Eurasian plate collision during early Eocene, resulted in the present-day configuration (Chatterjee et al. 2013; Burg 2011; Chatterjee and Scotese 2010; Khan et al. 2009; Ali and Aitchison 2008; Van der Voo et al. 1999; Reuber 1986). In addition, the tectonostratigraphic framework indicates that these shallow water carbonate platform deposits experienced burial from the late Cretaceous to early Eocene when collision of the India-Eurasia resulted in the uplifting of the area (Ahsan and Chaudhry 2008).

All the E-W oriented thrust faults found in the study area are the splays of the NE-SW Haro Thrust. It is evident that Samana Suk Formation (middle Jurassic) is thrusted over the Cretaceous Kawagrah Formation along most of these E-W trending splay thrusts (Fig. 1). These E-W oriented thrust faults may have provided pathways to Mg-rich fluids from the underlying siliciclastics (Chichali and Lumshiwal Formations) or from deep basinal fluids into the overlying studied carbonate successions. Multiple pulses of Mg-rich fluids may have been responsible for the relevant dolomite phases.

Diagenetic evolution and paragenetic sequence

A detailed paragenetic sequence of various diagenetic events has been established on the basis of field observations in conjunction with petrographic study (Fig. 10). The sharp limestone-dolomite contacts mostly cross-cutting stratification and sedimentary structures (bedding-parallel stylolites) suggest a late origin for the dolomites (Fig. 3c). Various generations of dolomite facies indicate multiple pulses of the dolomitizing fluids. Above mentioned E-W oriented splay faults provided pathways to Mg-rich fluids to accumulate first phase of medium to coarse crystalline dolomite Dol. I, followed by the formation of fine to medium crystalline dolomite (Dol. II). Furthermore, bedding-parallel stylolites (BPSs) documented in the replacive dolomite show burial conditions, which is also supported by the documentation of coarse to very coarse crystalline, nonplanar dolomite

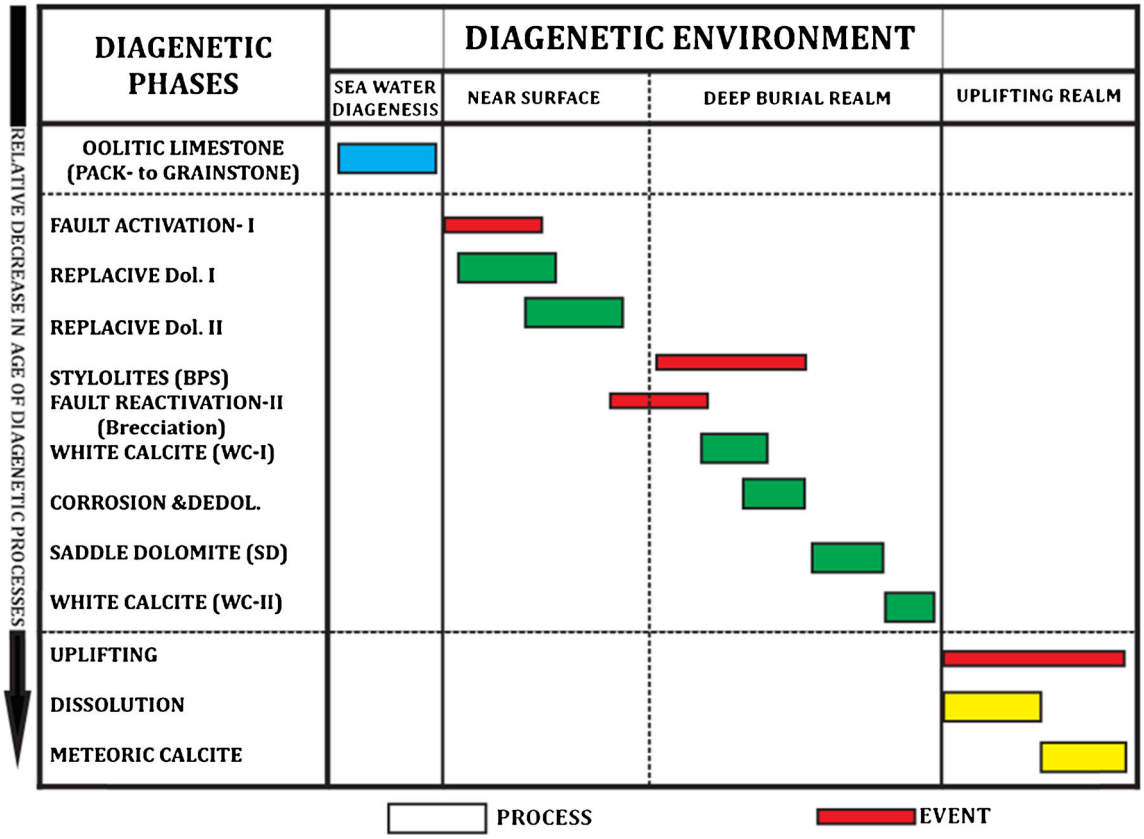

Fig. 10 Porosity-permeability studies of different dolomite phases showing porosity increase in matrix dolomite, whereas saddle dolomite exhibited low porosity-permeability values

that contains subhedral to euhedral crystals, showing undulose extinction (typical of saddle dolomite; Fig. 6e). Later, reactivation of faults resulted in the upwelling of calcite-rich fluids that resulted in white colored, dull orange luminescent calcite cement (WC-I) and caused intense brecciation of Dol. I (Fig. 3g). Possible explanation for the fragments to be "floating" would imply the involvement of very high fluid velocities, to render medium to coarse crystalline (millimeter to centimeter) dolomite fragments "buoyant" and an extremely rapid crystallization to "freeze" them in their floating position (Fig. 3g). Likewise, post-dolomite calcite cementation resulted in coarse crystalline, dull orange luminescent calcite (WC-II). On the basis of above mentioned observations, burial-associated phases include (i) SD, (ii) white calcite (WC-I), and (iii) white calcite (WC-II). The occurrence of dodecahedral crystals of pyrite up to 2 mm in diameter along the margins of pore-filled calcite suggests that some sulfidic fluids circulated in the system before the emplacement of WC-I (Fig. 6b). At the end of diagenetic history, late stage fracture- and vein-filling transparent, nonluminescent calcites post-date all the diagenetic phases and exhibit meteoric condition of formation (Choquette and James 1988; Niemann and Read 1988; Meyers 1991; Reeder 1991).

Stable isotope analyses of the host limestones close to the dolomites show depleted $\delta^{18}O$ values as compared to the original marine signatures, implying recrystallization during dolomitization (Fig. 8). First phase of replacive dolomite (Dol. I) represents relatively less depleted $\delta^{18}O$ signatures as compared to Dol. II, suggesting that Dol. II may have formed at relatively increased temperature as compared to Dol. I (Fig. 8). The reported $\delta^{13}C$ values of such replacive dolomites (Dol. I and Dol. II) are not far from the original marine signature of the host rocks (i.e., middle Jurassic); thus, the carbon isotopic composition of the dolomitizing fluids likely was buffered by the host rock. Furthermore, dolomite (SD) and calcite (WC-I and WC-II) cements also exhibit highly depleted $\delta^{18}O$ values. More depleted oxygen isotopic trend of dolomite cement SD (i.e., −12.17 to −12.43‰ V-PDB) may suggest that the fluids originated from greater depths with higher temperatures than the replacive dolomitizing fluids. Furthermore, various dolomite phases reveal a broad range of $d^{18}O$ values (i.e., between −12.43 and −3.91‰ V-PDB), which is consistent with multiphase dolomitization and dolomite recrystallization (Nielsen et al. 1994). All the observed diagenetic phases show deviation toward negative oxygen-isotope signatures, and increased temperature is the likely source of depleted $\delta^{18}O$ values. Late stage calcite shows depleted $\delta^{13}C$ values and may be interpreted as resulting from late telogenetic-diagenetic calcite fluids (Fig. 8).

Multiphase dolomitization model

In order to incorporate the tectonic history, field observations, petrographic studies, and isotopic signatures, it is argued that dolomitization occurred during Cenomanian-Ypresian time (i.e., after the deposition of Kawagarh Formation and before the Indian-Eurasian plate collision). This is because of the fact that similar dolomitization is also observed in the overlying middle Cretaceous Kawagarh Formation (Shah et al. submitted), whereas late dolomite and calcite phases are associated with hydrothermal realm (before uplift related to Indian-Eurasian collision). In particular, initial phase of dolomitization (Dol. I and Dol. II) resulted from the activation or reactivation of regional fault (i.e., Haro Thrust) and its splays in the study areas, which provided pathways for Mg-rich dolomitizing fluids from the deeper source. This is followed by further burial of the carbonate succession, which is evidenced by the presence of BPSs in the replacive dolomite, saddle dolomite, and dull orange luminescent calcite phases pre- and post-dating saddle dolomite. In the second stage, reactivation of faults resulted in the upwelling of hot and mobile calcite-rich fluids causing cataclastic deformation of Dol. I (Figs. 4d and 10). There are two possible sources of dolomitizing fluids, which include (i) burial-associated compactional dewatering of the dolomitizing fluids from deep basinal siliciclastics (i.e., Datta, Chichali, and Lumshiwal Formations) along the NE-SW trending Haro Fault and (ii) deep-sourced, Mg-rich hydrothermal fluids (Fig. 11). Furthermore, uplifting associated with continent-continent collision is manifested by the presence of transparent calcite representing meteoric recharge (Fig. 10).

Reservoir characterization

In general, the texture of the precursor limestone, dolomitizing fluid composition, and duration of dolomitization are the main factors that control the extent of dolomitization; thus, dolomitization may create, preserve, or diminish porosity depending on these stated parameters (Lucia and Major 1994). These different geometries suggest that the porosity, permeability, and mineral composition of the host limestone play an important role in the distribution, shape, and geometry of the dolomite geo-bodies (Murray and Lucia 1967; Bullen and Sibley 1984).

In the studied rocks, dolomite phase distribution controlled porosity evolution, which is evidenced by significantly high-

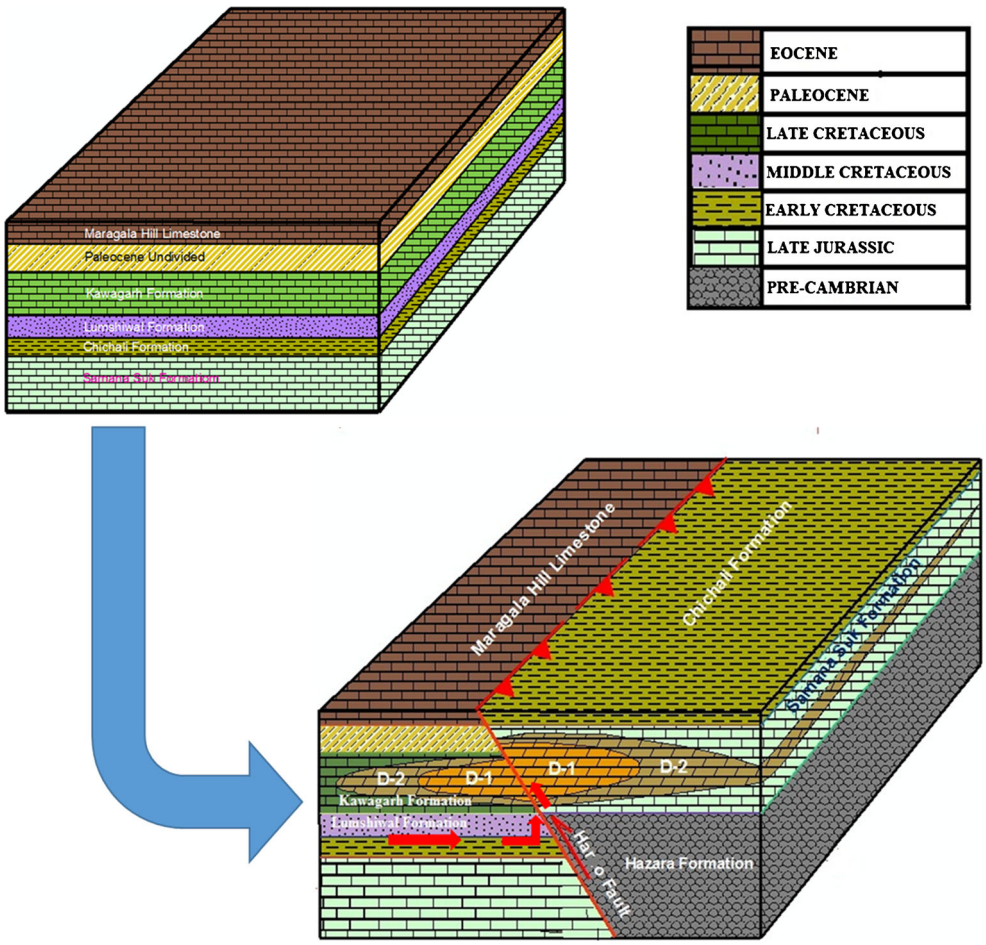

Fig. 11 Conceptual diagenetic model of the dolomite bodies in studied middle Jurassic platform carbonates

porosity and high-permeability values in the Dol. I (3.47 to 10.33 % and 1.36 to 8.97 mD), whereas Dol. II exhibited relatively lower porosity-permeability values (i.e., 3.14 to 4.56 % and 0.05 to 1.21 mD), respectively. This indicates that intercrystalline and fracture porosities, followed by cataclastic deformation, contributed toward high-porosity values in Dol. I, whereas low-porosity values of Dol. II and saddle dolomite are due to their interlocking nature of dolomite crystals (Fig. 8). In contrary, saddle dolomite exhibited relatively higher-permeability values as compared to Dol. II, and it may be due to the fact that interconnected pore spaces are clogged by early stage white calcite WC-I (i.e., before saddle dolomite emplacement). Diagenetic alterations also contributed toward porosity enhancement in the replacive dolomites. In addition, dissolution, brecciation, and/or cataclastic deformation greatly enhanced the petrophysical properties of studied dolomites (Fig. 3g). Conversely, late stage calcite and dolomite cementation reduced the porosity and permeability. Higher fracture intensity is observed in dolomite which postdates dolomitization.

Conclusions

Present study aims to investigate excellent exposure of fault-controlled bedding-parallel dolomite bodies in the middle Jurassic Samana Suk Formation, southern Hazara basin (NW Pakistan). On the basis of field observations, petrographic and mineralogical studies, isotopic analyses, and porosity/permeability studies of the above mentioned dolomite geobodies, following main points are deduced:

1. A comprehensive paragenetic sequence is established, which helped in understanding the diagenetic evolution of the various studied dolomite and calcite phases. Initial phase of replacive dolomitization (Dol. I and Dol. II) resulted from upwelling of hot Mg-rich fluids along the activated and/or reactivated splay faults of Haro Fault. Late phase of dolomitization emanated in SD. This is followed by the intense brecciation of Dol. I due to calcite-rich fluids and resulted in white calcite cement WC-I, followed by corrosion and dedolomitization of replacive dolomite. Finally, another episode of calcite cement (WC-II) post-dated calcite and dolomite phases. It is pertinent to mention that BPSs, calcite cement phases (WC-I and WC-II), and dolomite cement (SD) represented burial conditions. Late stage uplifting resulted in the formation of transparent calcite veins representing meteoric origin.
2. On the basis of O/C stable isotope signatures, Dol. II may have formed at relatively increased temperature as compared to Dol. I, whereas fluids responsible for the formation of dolomite and white calcite cements emanated from deep-buried conditions. Furthermore, the carbon isotopic composition of the dolomitizing fluids likely was buffered by the host rock. Besides, calcite (WC-I) and dolomite cement (SD) cements exhibit highly depleted $\delta^{18}O$ values as compared to calcite (WC-II). The stable isotope analyses reveal a broad range of $\delta^{18}O$ values mainly between −12.43 and −3.91‰ (V-PDB) and justify multiphase dolomitization. All the observed diagenetic phases show deviation toward negative oxygen-isotope signatures, and increased temperature is the likely reason to explain the depleted $\delta^{18}O$ values. Other depleted $\delta^{13}C$ values may be interpreted as resulting from late telogenetic calcite phase.
3. Conceptual dolomitization model suggests that multiphase dolomitization occurred in three phases. Initially, replacive dolomite (i.e., Dol. I and Dol. II) resulted in the reactivation of faults, followed by burial resulted in formation of SD and compactional dewatering of calcite-rich fluids along the NE-SW trending Haro Fault, and its E-W trending splays resulted in the accumulation of WC-I and WC-II. Finally, uplifting resulted in the precipitation of calcite related to meteoric origin. The major contributor to the dolomitizing fluids is probably deep basinal siliciclastic, in which the trapped marine water is the likely source for Mg-rich dolomitizing fluids. Other possible source can be deep-seated hydrothermal fluids circulated along the reactivated faults.
4. Replacive dolomitization, brecciation, and dissolution mostly contributed in the increase of porosity and permeability, but dolomite and calcite cementation adversely affected the reservoir behavior of the studied dolomite rocks.

References

Ahsan N, Chaudhry MN (2008) Geology of Hettangian to middle Eocene rocks of Hazara and Kashmir Basins, Northwest Lesser Himalayas. Pakistan Geol Bull Punjab Univ 43:131–152

Ali JR and Aitchison J (2008) Gondwana to Asia: plate tectonics, paleogeography and the biological connectivity of the Indian sub-continent from the Middle Jurassic through latest Eocene (166–35 Ma). 88(3–4), 145–166

Angiolini L, Balini M, Garzanti E, Nicora A, Tintori A (2003) Gondwana deglaciation and opening of neotethys: the Al Khlata and Saiwan Formations of interior Oman. Palaeogeogr Palaeoclimatol Palaeoecol 19:699–123

Bullen SB, Sibley DF (1984) Dolomite selectivity and mimic replacement. Geology 12:655–658

Burg JP (2011) The Asia-Kohistan-India collision: review and discussion. In: Brown D, Ryan PD (eds) Arc-Continent Collision, Frontiers in Earth Sciences. Springer-Verlag, Berlin, pp. 279–309

Calkins JA, Offield T W and Abdullah SKM (1975) Geology of the Southern Himalayas in Hazara, Pakistan and adjacent areas. Geological Investigation in Pakistan. p.124

Chatterjee S, Scotese CR (2010) The wandering Indian plate and its changing biogeography during the late Cretaceous-early Tertiary period. Ed. New Aspects of Mesozoic Biodiversity. Lect Notes Earth Sci 132:105–126

Chatterjee S, Goswami A, Scotese CR (2013) The longest voyage: tectonic, magmatic, and paleoclimatic evolution of the Indian plate during its northward flight from Gondwana to Asia. Gondwana Res 23:238–267

Chaudhry MN, Ahsan N, and Ghazanfar M (1998) A preliminary account of sedimentology of Hazara Basin from Jurassic to Eocene: Abstract volume 13th Himalaya-Karakoram-Tibet Workshop, Peshawar, pp. 41–43

Choquette PW, James NP (1988) Introduction. In: James NP, Choquette PW (eds) Paleokarst. Springer-verlag, New York, pp. 1–21

Coward MP, Butler RWH, Chambers AF, Graham RH, Izatt CN, Khan MA, Knipe RJ, Prior DJ, Treloar PJ, Williams MP (1988) Folding and imbrications of the Indian crust during the Himalayan collision. Philos Trans R Soc Lond A326:89–116

Davies GR, and Smith LB Jr (2006) Structurally controlled hydrothermal dolomite reservoir facies: An overview. AAPG Bulletin, 90(11): 1641–1690

Dewit J, Huysmans M, Muchez P, Hunt DW, Thurmond JB, Verges J, Saura E, Fernandez N, Romaire I, Esestime P, Swennen R (2012) Reservoir characteristics of fault controlled hydrothermal dolomite bodies: Ramales Platform case study. In: Garland J, Neilson JE, Laubach SE, Whidden KJ (eds) Advances in Carbonate Exploration and Reservoir Analysis, Geological Society of London. Special Publications 370, London, pp. 83–109

Dickson JAD (1966) Carbonate identification and genesis as revealed by staining. J Sediment Petrol 36:491–505

Ferrill DA, Morris P, Evans MA, Burkhard M, Groshong RH, Onasch CM (2004) Calcite twin morphology: a low-temperature deformation geothermometer. J Struct Geol 26(8):1521–1529

Fursich FT, Callomon JH, Pandey DK, Jaitly AK (2004) Environments and faunal pattern in the Kachh Rift Basin, western India, during Jurassic. Riv Ital Paleontol Stratigr 110:181–190

Garzanti E (1993) Sedimentary evolution and drowning of a passive margin shelf Giumal Group; Zanskar Tethys Himalaya, India: palaeoenvironmental changes during final break-up of Gondwanaland, in P.J. Treloar and M.P. Searle, eds. Himalayan Tectonics. Geol Soc Spec Pub 74:277–298

Gomez-Rivas E, Corbella M, Martín-Martín JD, Stafford SL, Teixell A, Bons PD, Cardellach E (2014) Reactivity of dolomitizing fluids and Mg source evaluation of fault-controlled dolomitization at the Benicassim outcrop analogue (Maestrat Basin, E Spain). Mar Pet Geol 55:26–42

Gonzales-Casado JM, Garcia-Cuevas C (1999) Calcite twins from microveins as indicators of deformation history. J Struct Geol 21: 875–889

Hendry JP, Gregg JM, Shelton KL, Somerville ID, Crowley SF (2015) Origin, characteristics and distribution of fault-related and fracture-related dolomitization: insights from Mississippian carbonates. Isle Of Man, Sedimentology 62:717–752

Kazmi, AH and Jan MQ (1997) Geology and tectonics of Pakistan. Graphic Publishers Pakistan, 554

Khan SD, Walker DJ, Hall SA, Burke KC, Shah MT, Stockli L (2009) Did Kohistan-Ladakh island arc collide first with India? Geol Soc Am Bull 121:366–384

Lacombe O (2010) Calcite twins, a tool for tectonic studies in thrust belts and stable orogenic forelands. Oil & Gas Science and Technology–rev. IFP Energies Nouvelles 65(6):809–838

Lacombe O, Amrouch K, Mouthereau F, Dissez L (2007) Calcite twinning constraints on late Neogene stress patterns and deformation mechanisms in the active Zagros collision belt. Geology 35(3): 263–266

Lee T, Lawver LA (1995) Cenozoic plate reconstruction of Southeast Asia. Tectonophysics 251(1–4):85–138

Lopez-Horgue MA, Iriarte E, Schroder S, Fernandez-Mediola PA, Caline B, Corneyllie H, Fremont J, Sudrie M, Zerti S (2010) Structurally controlled hydrothermal dolomites in Albian carbonates of the Ason Valley, Basque Cantabrian Basin. Northern Spain Mar Pet Geol 27(5):1069–1092

Lucia, F. J. and Major, R. P. (1994). Porosity evolution through hypersaline reflux dolomitization. In: Purser, B. H., Tucker, M. E and Zenger, D. H. Eds, Dolomites, a volume in honor of Dolomieu. Int. Assoc. Sedimentology. Spec. Publ. 21, 325–341.

Lumsden DN (1979) Discrepancy between thin section and X-ray estimates of dolomite in limestone. J Sediment Petrol 49:429–436

Martín-Martín JDA, Trave A, Gomez-Rivas E, Salas R, Sizun JP, Verges J, Corbella M, Stafford SL, Alfonso P (2015) Fault-controlled and stratabound dolostones in the Late Aptian-earliest Albian Benassal Formation (Maestrat Basin, E Spain): petrology and geochemistry constrains. Mar Pet Geol 65:83–102

McKenzie D, Sclater JG (1971) The evolution of the Indian Ocean since the Late Cretaceous. Geophys J Int 24(5):437–528

Meyers WJ (1991) Calcite cement stratigraphy. In: C.E. Baker and O.C. Kopp (eds), luminescence microscopy and spectroscopy: qualitative and quantitative aspects. SEPM Short Course 25:133–148

Murray RC, Lucia FJ (1967) Cause and control of dolomite distribution by rock selectivity. Geol Soc Am Bull 78:21–35

Nader FH, Dumont C, Shah MM, Garcia D, Swennen R, Daniel J-M, Lerat O, and Doligez B (2009) From field study to numerical modelling of hydrothermal dolomitization in Early Cretaceous platform carbonates (Cantabrian mountains, northern Spain). J Geochem Explor, 101, pp. 73

Nielsen P, Swennen R, Keppens E (1994) Multiple-step recrystallization within massive ancient dolomite units: an example from the Dinantian of Belgium. Sedimentology 41:567–584

Niemann JC, Read JF (1988) Regional cementation from unconformity-recharge aquifer and burial fluids. Mississipian Newman Limestone, Kentucky. J Sed Petrol 58:688–705

Patriat P, Achache J (1984) India-Eurasia collision chronology and its implications for crustal shortening and driving mechanisms of plates. Nature 311:615–621

Radke BM, Mathis RL (1980) On the formation and occurrence of saddle dolomite. J Sediment Res 50(4):1149–1168

Reeder RJ (1991) An over-view of zoning in carbonate minerals. In: C.E. Baker and O.C. Kopp (Eds), luminescence microscopy and spectroscopy: Qualitative and quantitative aspects. SEPM short course 25, pp. 77–82

Reuber I (1986) Geometry of accretion and oceanic thrusting of the Spongtang ophiolite, Ladakh-Himalaya. Nature 321:592–596

Rosenbaum J, Sheppard SM (1986) An isotopic study of siderites, dolomites and ankerites at high temperatures. Geochim Cosmochim Acta 50:1147–1150

Rowley DB (1996) Age of initiation of collision between India and Asia: a review of stratigraphic data. Earth Planetary Lett 145:1–13

Searl A (1989) Saddle dolomite: a new view of its nature and origin. Mineral Mag 53(5):547–555

Sengor, A. M. C., Altiner, D., Cin, A., Ustaomer, T. and Hsu, K.J. (1988). Origin and assembly of the Tethyside orogenic collage at the expense of Gondwanaland. In: Audley-Charles, M.G. & Hallam, A. Eds. Gondwana and Tethys. Geol. Soc. Lond., Spec Publ 37: 81–119.

Shah SMI (1977) Stratigraphy of Pakistan. Geol Surv Pakistan, Quetta, Mem Geol Surv 12:138

Sharp I, Gillespie P, Morsalnezhad D, Taberner C, Karpuz R, Verges J, Horbury A, Pickard N, Garland J, Hunt D (2010) Stratigraphic architecture and fracture-controlled dolomitization of the Cretaceous Khami and Bangestan groups: an outcrop case study, Zagros Mountains, Iran. In: van Buchem FSP, Gerdes KD,

Esteban M (eds) Mesozoic and Cenozoic Carbonate Systems of the Mediterranean and the Middle East: Stratigraphic and Diagenetic Reference Models. Geol. Soc, Lond. Sp. Publ. 329, London, pp. 343–396

Sibley DF, Gregg JM (1987) Classification of dolomite rock textures. J Sediment Petrol 57:967–975

Van der Voo R, Spakman W, Bijwaard H (1999) Tethyan subducted slabs under India. Earth Planet Sci Lett 171:7–20

Vandeginste V, John CM, Cosgrove JW, Manning C (2014) Dimensions, texture distribution, and geochemical heterogeneities of fracture-related dolomite geobodies hosted in Ediacaran Limestones, Northern Oman. AAPG Bull 98(9):1789–1809

Wachter E and Hayes JM (1985) Exchange of oxygen isotopes in carbon-dioxidephosphoric acid systems. Chem Geol, 52, 365–374

Yeats RS, Hussain A (1987) Timing of structural events in the Himalayan foothills of northern Pakistan. J Geol Soc London 153:677–680